Journal of Applied Polymer Science

Pullulan: A versatile coating agent for superparamagnetic iron oxide nanoparticles

Sergiu Coseri,[1] Alina Spatareanu,[1] Liviu Sacarescu,[1] Vlad Socoliuc,[2] Ioan Sorin Stratulat,[1,3,4] Valeria Harabagiu[1]

[1]Petru Poni Institute of Macromolecular Chemistry of Romanian Academy, 41A Grigore Ghica Voda Alley 700487, Iasi, Romania

[2]Laboratory of Magnetic Fluids, Center for Fundamental and Advanced Technical Research, Romanian Academy–Timisoara Branch, 24 Mihai Viteazul Boulevard 300223, Timisoara, Romania

[3]Faculty of Medicine, Grigore T. Popa University of Medicine and Pharmacy, Iasi, Romania

[4]Romanian Railroad Clinic Hospital Iasi, Rehabilitation, Physical Medicine, and Balneoclimatology Clinic (Caile Ferate Romane Hospital), Iasi 700506, Romania

Correspondence to: S. Coseri (E-mail: coseris@icmpp.ro)

ABSTRACT: Ultrasmall superparamagnetic iron oxide (Fe_3O_4) nanoparticles coated by biocompatible pullulan (Pu-USPIO) with sizes below 10 nm and having a magnetite core and a hydrophilic outer shell of pullulan were prepared. The formed Pu-USPIOs were thoroughly characterized by Fourier transform infrared spectroscopy, transmission electron microscopy, atomic force microscopy, and small-angle X-ray scattering experiments. The content of magnetic nanoparticles embedded into the pullulan matrix was determined by thermogravimetric analysis. Vibrating sample magnetometry analysis was used to evaluate the magnetic properties of the Pu-USPIO samples. Because of the presence of pullulan, these nanoparticles could be conditioned in many versatile forms, from a clear solution to magnetic films, for potential applications, including magnetic hyperthermia mediators. © 2015 Wiley Periodicals, Inc. J. Appl. Polym. Sci. **2016**, *133*, 42926.

KEYWORDS: magnetism and magnetic properties; nanoparticles; nanowires and nano crystals; polysaccharides; properties and characterization

Received 7 July 2015; accepted 10 September 2015

DOI: 10.1002/app.42926

INTRODUCTION

Pullulan is a water-soluble polysaccharide produced by the yeastlike fungus *Aureobasidium pullulans*. It has been well established that regularly repeating structural unit of pullulan is a maltotriose trimer [α-(1→4)Glucopyranosyl-α-(1→4)Glu*p*-α-(1→6)Glu*p*— (Figure 1).[1] Pullulan has numerous applications, including ones in the food industry, health care, pharmaceuticals, and medicine. In the last decade, pullulan has received a lot of attention as useful candidate for use in various medicine applications because of its biocompatibility, nontoxicity, and water solubility. We very recently reported the use of pullulan and its C-6 oxidized analogue for silver nanoparticle preparation under environmentally friendly conditions with excellent antibacterial activities against both Gram-positive and Gram-negative bacterial strains.[2]

Nowadays, iron oxide (Fe_3O_4) superparamagnetic nanoparticles represent a hot topic in research, and they have found various utilizations in high-tech applications in chemistry and biomedical fields; these include applications in catalysts, hyperthermia, magnetic resonance imaging, bioseparation, diagnostic agents, biomolecule immobilization, and drug delivery.[3,4] For the medical application of magnetic nanoparticles, properties such as biocompatibility, biodegradability, and long-term stability are highly required. Because of their hydrophobic surface and large surface-area-to-volume ratio, the use of iron oxide nanoparticles *in vivo* is limited because of their rapid clearance from the circulation by the reticuloendothelial system.[5] To circumvent this obstacle, one approach is to use highly hydrophilic coating materials to considerably prolong the nanoparticle half-life in the circulation.[6] Iron oxide nanoparticles usually have a high affinity for gathering together. However, polysaccharide matrices can prevent this phenomenon because they act as stabilizers.[7] Therefore, the main objectives of our research were to prepare and characterize surface-modified ultrasmall superparamagnetic iron oxide nanoparticles coated by pullulan (Pu-USPIO) as a coating agent. Pullulan has several advantages for this purpose: a high water solubility and hydrophilicity, a lack of toxicity,

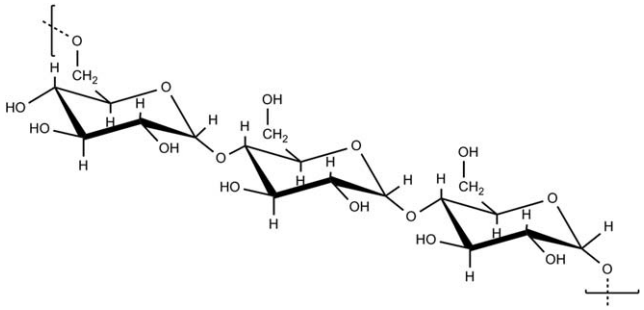

Figure 1. Chemical structure of pullulan.

safety for human use (it is already used as a food additive), nonimmunogenicity, and nonantigenicity.[8] Moreover, there is evidence for the receptor-mediated hepatic uptake of pullulan.[9] Ultrasmall superparamagnetic iron oxide nanoparticles refer to magnetic iron oxide nanoparticles that are smaller than 50 nm.[10] These particles, because of their properties and size, can be used for tracing cells and tumors *in vivo*.[10,11] Chitosan and carboxymethyl chitosan are other two polysaccharides that are used to prepare magnetic nanoparticle dispersions.[12,13] Recently, other polysaccharides, such as soluble starch, carboxymethylcellulose sodium, and agar, have found applications as stabilizers in the synthesis of magnetic Fe_3O_4 nanoparticles.[14] It is well known that magnetic nanoparticles are often stabilized with oleic acid. In this way, these nanoparticles can be used in various applications; this prevents their agglomeration. In this study, pullulan was used to replace the oleic acid and to take over its stabilizing properties. The scope of this exchange between stabilizers could be beneficial for application of magnetic nanoparticles in the areas of biology and biomedicine because of the exceptional properties of pullulan in these fields.

EXPERIMENTAL

Materials

Pullulan (weight-average molecular weight = 150 kDa) purchased from TCI Europe was dried *in vacuo* at 100°C overnight before use. Ethanol (EtOH) was analytical grade and was used without any further treatment. Distilled water (chromatographic purity) was used for the preparation of the pullulan solutions and magnetite–pullulan mixtures.

Synthesis of Oleic Acid Coated Magnetic Nanoparticles

The preparation of the oleic acid coated magnetic nanoparticles was accomplished by the Center for Fundamental and Advanced Technical Research, Romanian Academy, Timisoara Branch, Romania. The procedure followed a recipe that was previously published.[15–17] Namely, $FeSO_4{\cdot}7H_2O$ and $FeCl_3{\cdot}4H_2O$ salts were used for the coprecipitation of Fe^{2+} and Fe^{3+} ions in the presence of an NH_4OH aqueous solution at 80–82°C. Once the coprecipitation had started, oleic acid was added in significant excess (ca. 30 vol %) to the system; this resulted in the chemisorption of the oleic acid on the magnetite surface. The thus-formed nanoparticles were washed several times with distilled water with magnetic decantation and filtration to remove the aggregated (nondispersed) particles. Flocculation (acetone) was used to extract the magnetite particles coated with a single surfactant layer from the solution of residual salts and free surfactant.

Pu-USPIO Preparation

The oleic acid coated magnetic nanoparticles previously fabricated were used to prepare Pu-USPIOs. A certain amount of magnetite nanoparticles, corresponding to 0.05, 0.1, 0.5, and 5% (wt) concentrations, were dispersed in 20 mL of EtOH and vigorously stirred. After 2 h, EtOH was carefully removed and replaced by another portion of fresh EtOH; we continued the stirring for another 6 h. EtOH was replaced by distilled water, and the resulting dispersion was sonicated at 9000 rpm (at 50 W for 30 min). To this solution, 50 mL of a 1% w/v pullulan aqueous solution was added dropwise. The resulting mixture was again sonicated for another 15 min at 12,000 rpm (at 50 W), and this was followed by centrifugation. The supernatant was collected and used to obtain the Pu-USPIO films by evaporation of the solvent *in vacuo* at 60°C for 48 h.

Characterization

Fourier Transform Infrared (FTIR) Spectroscopy. The FTIR spectra of the pullulan and superparamagnetic iron oxide nanoparticle samples were recorded with a Bruker Vertex 70 spectrometer in a scan range from 4000 to 650 cm^{-1} at a resolution of 2 cm^{-1} for 32 scans. The dried samples was powdered by grinding with KBr pellets and pressed into a mold.

Morphological Observations. Transmission electron microscopy (TEM) images were acquired with a Hitachi High-Tech HT7700 electron microscope (Hitachi High-Technologies Corp., Tokyo, Japan) with a drop of Pu-USPIO aqueous solution placed directly onto a carbon-coated copper grid. We allowed this to dry before TEM analysis. The particle size distribution was evaluated with the UTHSCSA Image Tool Version 3.00 program (UTHSCSA Dental Diagnostic Science, San Antonio, TX). The energy-dispersive X-ray (EDX) analysis was performed on a Quanta 200 (FEI) electron microscope equipped with an EDX system. The operated voltage was 30 kV, and the current was 36 mA.

Topographical features of the surfaces were characterized with atomic force microscopy (AFM) in tapping mode with an Agilent 5500 AFM multimode scanning probe microscope (Digital Instruments, Santa Barbara, CA). The images were scanned with silicon cantilevers (ATEC-NC, Nanosensors, Germany) with a resonance frequency of 210–490 kHz and a force constant of 12–110 N/m. All of the measurements were performed at ambient temperature in air.

The Quanta 200 microscope, operating at 20 kV and equipped with an EDX system was used for qualitative and quantitative analysis and elemental mapping.

Small-angle X-ray scattering (SAXS) experiments were performed on a Nanostar U-Bruker system equipped with a Vantec 3000 detector (diameter = 200 mm) and an X-ray I μS microsource. The wavelength of the incident X-ray beam was 1.54 Å (Cu Kα), and the beam was collimated by three pinholes. The sample-to-detector distance was 107 cm; this allowed measurements with scattering vector (q) values between 0.01 and 0.15 $Å^{-1}$. The angular scale was calibrated by the scattering peaks of a silver behenate standard. The samples under study were deposited on Scotch tape and measured *in vacuo* with a dedicated holder at a constant temperature of 25°C. The Scotch tape

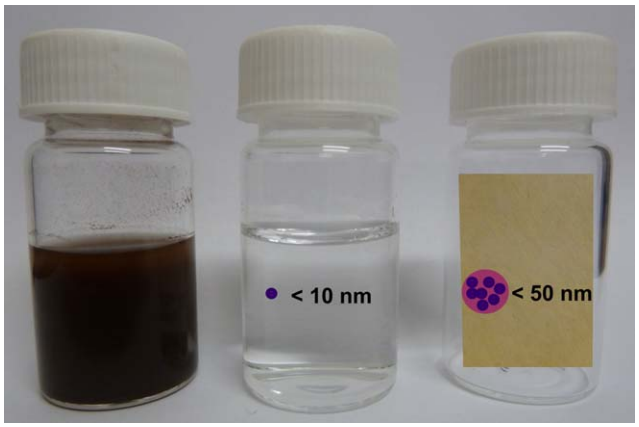

Figure 2. Photographs of the pullulan–magnetite mixture before centrifugation (left), after centrifugation (center), and after film formation (right). [Color figure can be viewed in the online issue, which is available at wileyonlinelibrary.com.]

and empty beam background was subtracted from the original intensity profiles. The data analysis was done with SAXS-NT (Bruker Integrated) and ATSAS 2.5.1 software.

Dynamic Light Scattering (DLS) Analysis. The ζ potential was measured with a DLS technique (Zetasizer model Nano ZS, Malvern Instruments, United Kingdom) with red laser at 633 nm (He–Ne). The average particle size was also measured on the basis of the DLS analysis.

The ζ potential was calculated from the electrophoretic mobility (μ) determined at 25°C. For $k\alpha \gg 1$ (where k is the Debye–Huckel parameter and α is the particle radius), the Smoluchowski relationship was used:

$$\xi = \eta\mu/\varepsilon \quad (1)$$

where η is the viscosity and ε is the dielectric constant.

Thermogravimetric Analysis (TGA)

A thermal analyzer (STA 449 F1 Jupiter device, Netzsch, Germany) was used to determine the weight loss percentage of the coated and uncoated magnetite nanoparticles. Samples (ca. 10 mg) were placed in Al_2O_3 crucibles and heated under nitrogen from 30 to 700°C at a 10°C/min heating rate. Thermogravimetry and derivative thermogravimetry (DTG) curves recorded with a ±0.5°C precision were analyzed with Netzsch Proteus analysis software.

Magnetic Properties

The magnetization of the samples was measured by means of vibrating sample magnetometry (VSM) with an ADE Technologies VSM 880 instrument. The magnetization curves of the samples were measured at room temperature in the field range 0–1000 kA/m.

RESULTS AND DISCUSSION

Preparation and Characterization of the Pu-USPIO Samples

Several samples of pullulan-coated superparamagnetic nanoparticles were prepared with magnetic Fe_3O_4 nanoparticles coated with oleic acid. To remove the stabilizer (oleic acid), these nanoparticles were washed several times with EtOH and distilled water. Four concentrations of Fe_3O_4 nanoparticles were used: 0.05, 0.1, 0.5, and 5% w/v (see the Experimental section). After sonication, these dispersions were independently mixed with 1% w/v aqueous pullulan. The obtained samples were denoted as PuF_x, where x is the initial concentration of the Fe_3O_4 nanoparticles used. However, the final (actual) concentration of the Fe_3O_4 nanoparticles encapsulated by pullulan was rigorously determined with magnetization experiments and TGA (see later). Figure 2 shows photographs of the pullulan–magnetite mixture before and after centrifugation and the obtained pullulan–magnetite films.

As shown in Figure 2, after centrifugation and the separation of the sediment, the resulting supernatant, which contained a pullulan solution with magnetite nanoparticles, appeared as a clear, homogeneous, transparent solution. The residual (solid) fraction resulting from centrifugation was put aside and used for different kinds of applications. For the medical application that we envisaged, the homogeneous and transparency solution was reclaimed; this solution still contained quite a high number of nanoparticles. Because of its physical properties, this solution could be used for applications when injection protocols were needed. Furthermore, the clear solution was used for the preparation of the pullulan–magnetite nanoparticles films through the addition of 5 mL of this solution to a Petri dish followed by the evaporation of the solvent (water) for 24 h at 60°C in a vacuum oven. In this way, we obtained another conditioning form of the magnetite nanoparticles.

FTIR Spectroscopy

The pullulan–magnetite nanoparticles were first analyzed by FTIR spectroscopy. The characteristic band located at around 585 cm^{-1} of Fe—O vibrations[18,19] in magnetite was present in all of the pullulan–magnetite samples but shifted to higher wave numbers; this indicated that surface complexation occurred. All of the FTIR spectra are shown in Figure 3. The main absorption band of the pullulan as a coating material were observed at

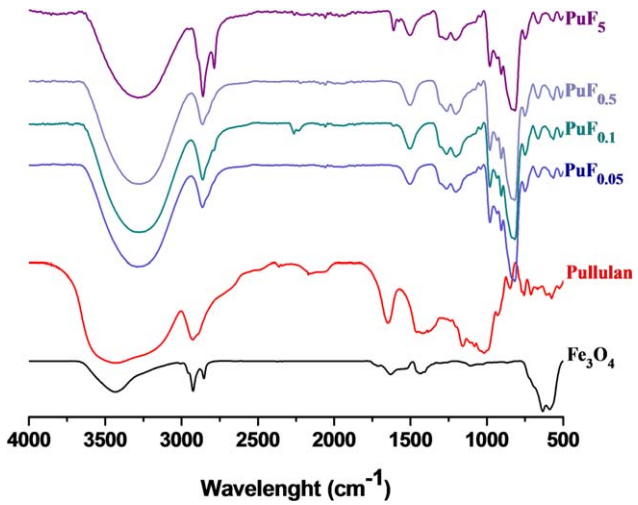

Figure 3. FTIR spectra of the magnetite, pullulan, and resulting PuF_x nanoparticles. [Color figure can be viewed in the online issue, which is available at wileyonlinelibrary.com.]

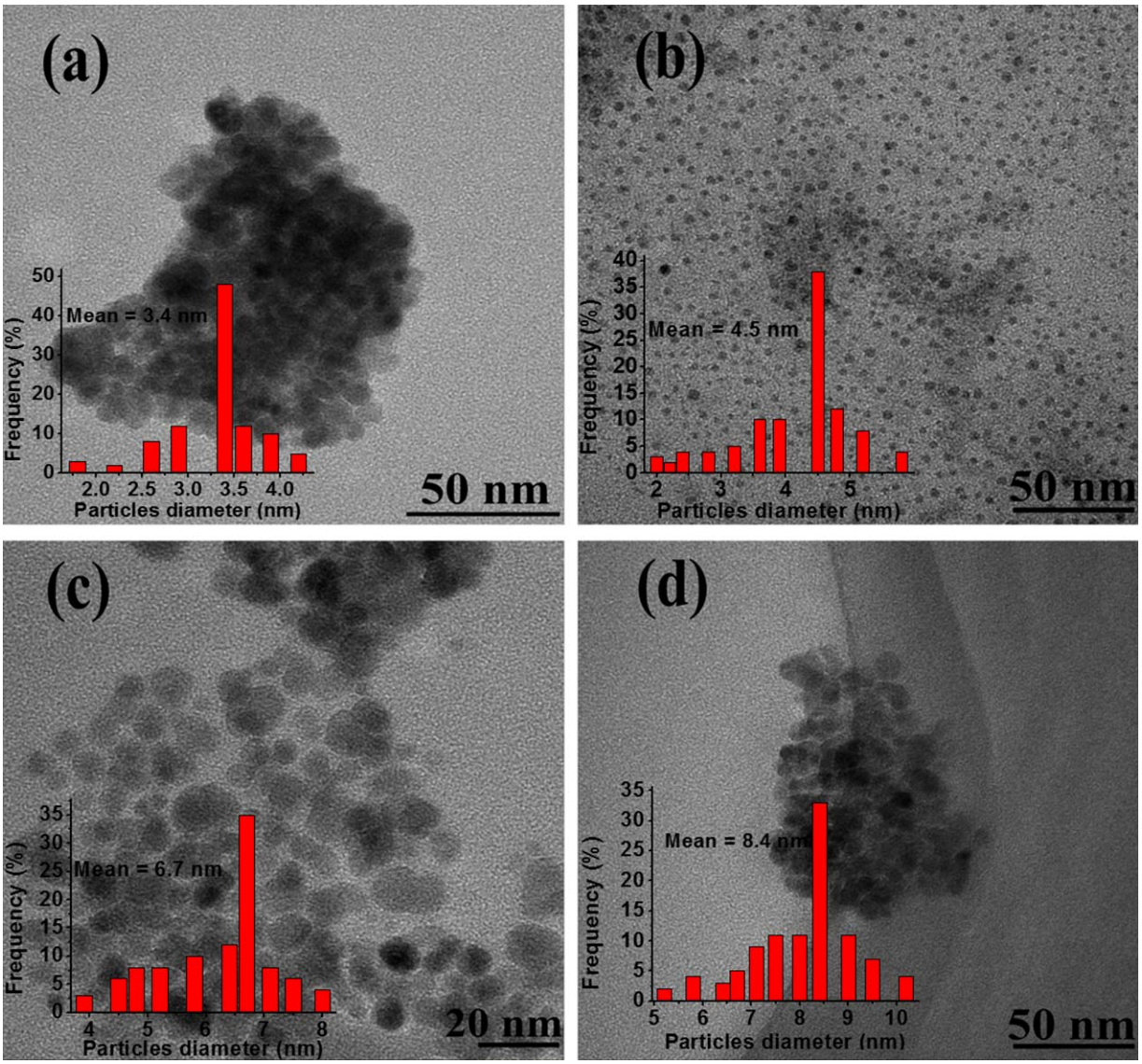

Figure 4. TEM images of the (a) $PuF_{0.05}$, (b) $PuF_{0.1}$, (c) $PuF_{0.5}$, and (d) PuF_5 samples. [Color figure can be viewed in the online issue, which is available at wileyonlinelibrary.com.]

3421 cm^{-1}; this arose from the stretching vibrations of the hydroxyl groups. Also, the signals observed at 1025 and 1647 cm^{-1} were due to the C—CO and C═O stretching modes. The bands from 2930 and 980 cm^{-1} originated from —CH_2 stretching vibrations and —CH out-of-plane bending vibrations, respectively. After the incorporation of the iron nanoparticles into the pullulan matrix (samples PuF_x), these adsorption bands were slightly shifted toward lower wavelengths; this indicated that pullulan was coated on the surface of the magnetic nanoparticles. Moreover, the peaks at 710, 756, 850, and 932 cm^{-1} may also have originated from iron oxide lattice deformation and OH groups bound on the surface of the Fe_3O_4 nanoparticles.[20]

Morphological Observations

The shape, size, and degree of uniformity of the iron nanoparticles were studied by means of TEM, AFM, and SAXS. The TEM technique provided information about the shapes and sizes of the nanoparticles. As shown in Figure 4, the pullulan-coated magnetic nanoparticles were nearly spherical in shape and were well separated in all cases. The average sizes of the particles as determined by TEM through the measurement of the size of about 200 particles were situated for all of the samples below 10 nm and were as follows: 3.4 ± 0.2 nm (sample $PuF_{0.05}$), 4.5 ± 0.3 nm (sample $PuF_{0.1}$), 6.7 ± 0.3 nm (sample $PuF_{0.5}$), and 8.4 ± 0.4 nm (sample PuF_5); this suggested that the nanoparticles size increased with increasing starting concentration of the magnetite.

Additionally, the particles were analyzed by AFM. The AFM images are presented in Figure 5. As shown by the AFM images, the magnetite nanoparticles had a strong tendency to agglomerate in the dry state; this depended on the initial concentration of the magnetite.

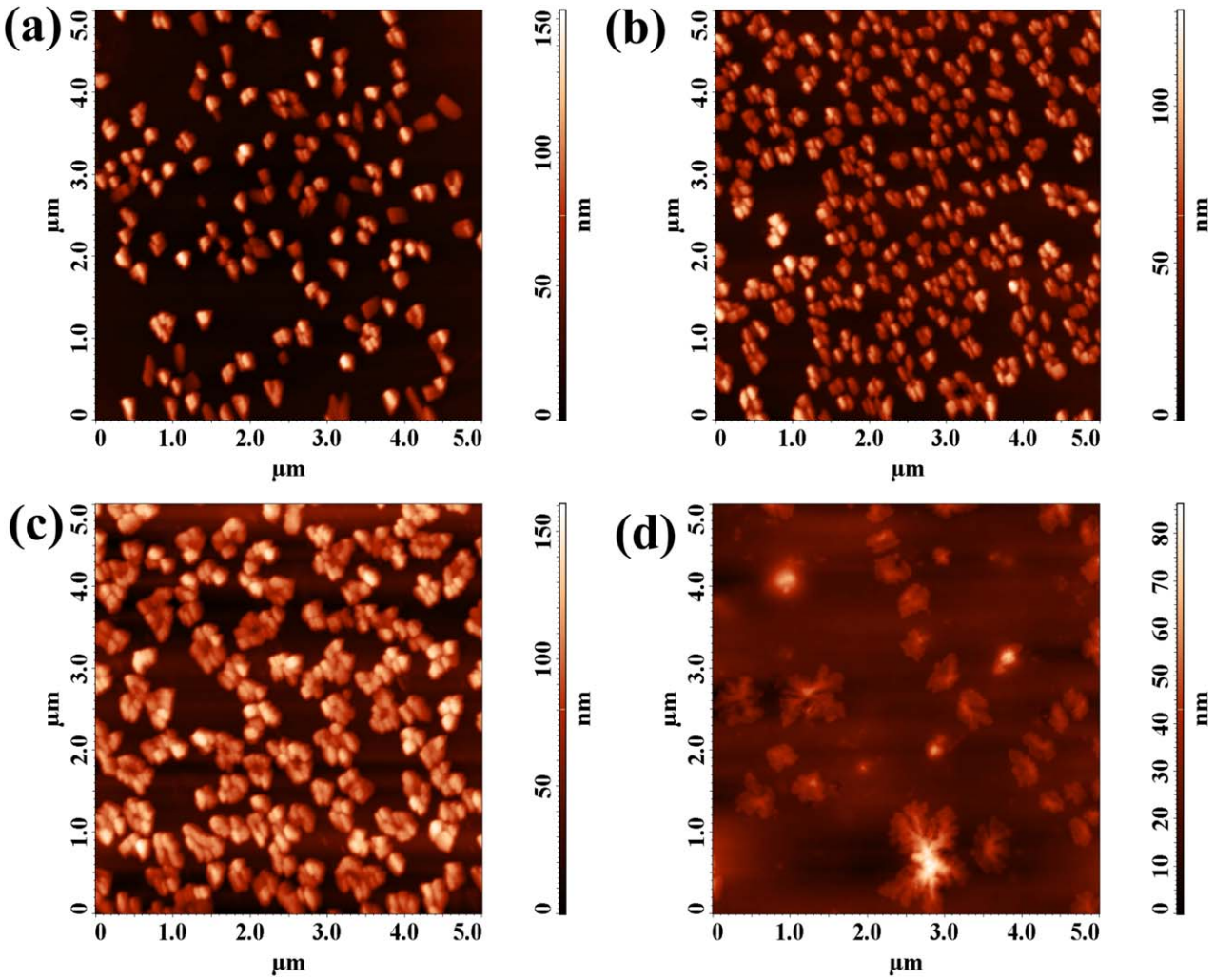

Figure 5. AFM images of the (a) $PuF_{0.05}$, (b) $PuF_{0.1}$, (c) $PuF_{0.5}$, and (d) PuF_5 samples. [Color figure can be viewed in the online issue, which is available at wileyonlinelibrary.com.]

The distribution of the magnetite nanoparticles was quite uniform in all of the samples; however, the cluster tended to become bigger and bigger once the magnetite concentration used for the film preparation increased. These clusters had sizes ranging from 20 nm for $PuF_{0.05}$ to 50 nm for PuF_5. It was clear that the sizes found with AFM experiments differed from those determined with the TEM technique. The differences could be explained by the sample preparation technique, which affected the obtained results; more precisely, the thermic treatment required for the pullulan–magnetite film preparation acted as a catalyst for cluster formation.

The scattering profiles for all of the studied samples were compared in log–log plots and Kratky plots. These representations suggest the characteristics of each sample (Figure 6).

Thus, it was clear that sample $PuF_{0.05}$ was a biphasic system with a low content in phase 1 (nanoparticles) and that this phase was highly dispersed within the matrix. The system was highly polydispersed (Kratky plot), and most of the nanoparticles were aggregated in clusters with a fractal geometry. A similar picture was observed for sample $PuF_{0.1}$ except its higher scattering intensity suggested a higher content in the nanoparticles (NP) clusters. This sample was highly polydisperse (Kratky plot), but the shape of the fractal clusters changed. On the other hand, the samples $PuF_{0.5}$ and PuF_5 presented a high

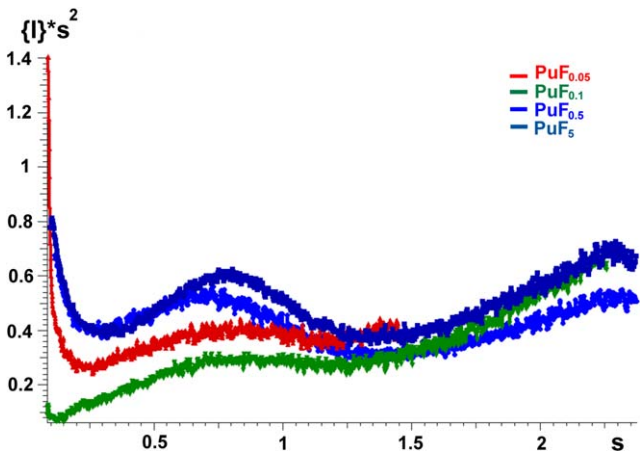

Figure 6. Kratky plots for the pullulan–magnetite samples. Scattering intensity (I), Structure factor (s). [Color figure can be viewed in the online issue, which is available at wileyonlinelibrary.com.]

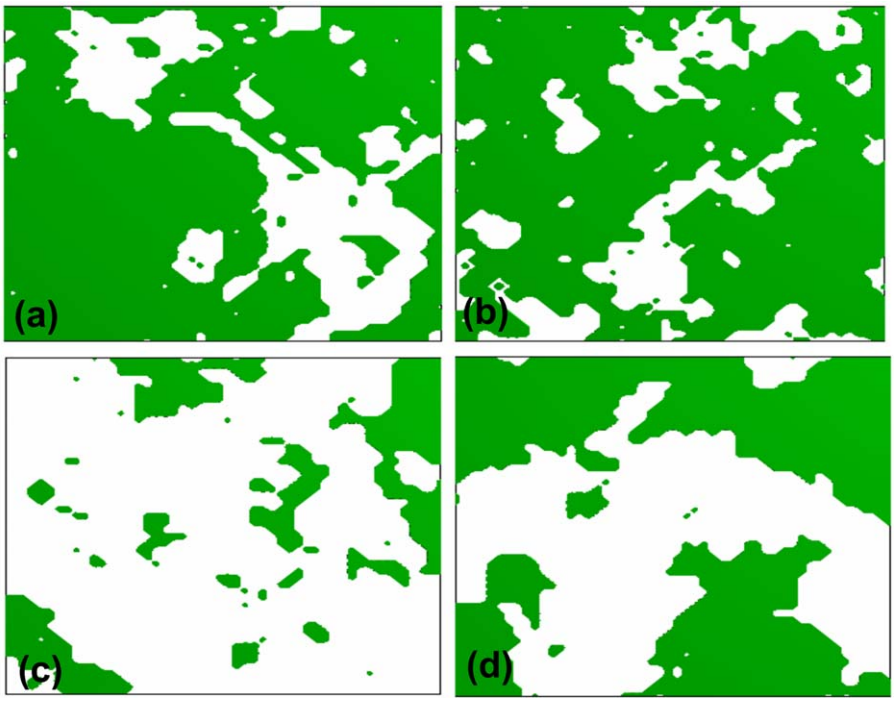

Figure 7. Phase morphology for the (a) $PuF_{0.05}$, (b) $PuF_{0.1}$, (c) $PuF_{0.5}$, and (d) PuF_5 samples. [Color figure can be viewed in the online issue, which is available at wileyonlinelibrary.com.]

similitude. These samples had a lower polydispersity (Kratky plot); this indicated that the NP clusters had almost the same dimensions (50 nm) and shape. These findings could be explained by the fact when lower concentrations of magnetite were used for the Pu-USPIO preparation, there was no tendency by the resulting nanoparticles to aggregate. Therefore, the size of the nanoparticles was much smaller than in the case when a higher concentration of magnetite was used, where the resulting nanoparticles were much more likely to aggregate and form clusters, which were seen as entities during SAXS analysis. Moreover, the differences occurred in the sample preparation for these techniques; that is, in TEM, we used a liquid sample for analysis, whereas in the SAXS and AFM analyses, we used films of pullulan–magnetite nanoparticles obtained by solvent evaporation at 60°C, when supplemental aggregation phenomena were expected.

Further considerations were concerned with the reconstruction of the phase morphology (Figure 7) with SAXSmorph software.

The morphology of the investigated samples showed particularities that were related mainly to the extent of the phase 1 (NP) continuity within the matrix. Therefore, sample $PuF_{0.5}$ showed a wide area (white) as a continuous phase built inside small domains of the scattered polymer matrix. Sample PuF_5, which showed similarities to sample $PuF_{0.5}$, had quite equal dispersed areas with a well-balanced distribution of particles inside the polymer matrix. The samples $PuF_{0.05}$ and $PuF_{0.1}$ contained scattered areas of NPs dispersed within the polymer matrix. The clusters were more like fractal geometry and was more compact for sample PuF_5. The dispersion of the clusters was different in each sample, with particularities that made possible the estimation of the NP phase dispersion within the polymer matrix.

The elemental composition of the pullulan–magnetite nanoparticles was determined by EDX. The incorporation of magnetite into the pullulan matrix was confirmed by the presence of the Fe signal, whereas other atomic signals (C, O) were derived from the polysaccharide matrix. The spatial distribution of the iron atoms from the mapping images of all of the analyzed samples revealed the uniform distribution of Fe atoms in the organic polymer (Figure 8).

The rather low content of Fe found in the EDX spectra was an indication that most of the magnetite nanoparticles were encapsulated in pullulan.

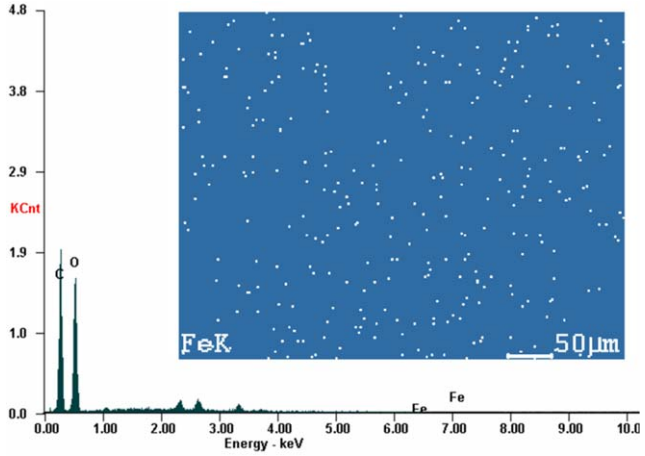

Figure 8. Typical EDX spectra of the pullulan–magnetite sample and iron elemental mapping (insert), X-ray intensity in kilocounts (KCnt), X-ray emitted by the Fe electrons in K shell (FeK). [Color figure can be viewed in the online issue, which is available at wileyonlinelibrary.com.]

Table I. Average Size Values (Determined by DLS at 25 ± 0.1°C), Polydispersity Indices, and ζ Potential Values of the PuF_x Samples at pH 6.5

Sample	Size (nm)	Polydispersity index	ζ potential (mV)
$PuF_{0.05}$	206	0.579	−0.75
$PuF_{0.1}$	209	0.620	−1.06
$PuF_{0.5}$	269	0.293	−1.21
PuF_5	273	0.254	−1.44

DLS Measurements

DLS measurements of the pullulan–magnetite samples were performed at room temperature and pH 6.5. The results are presented in Table I.

The sizes determined by DLS for the PuF_x samples differed from those determined with TEM or even the SAXS and AFM techniques. Also, the quality of the correlation functions was poor, as shown by the larger polydispersity indices in Table I. Therefore, these sizes seemed to be too large relative to data collected with other techniques.[21] The DLS measurements should be interpreted cautiously and could be useful for relative comparisons of the whole set of values. In fact, DLS measures the hydrodynamic size, and the calculated size cannot be considered as a real value because there is always a tendency to overestimate the real size because of the strong interactions between solvent and nanoparticles constituents, especially for hydrophilic biopolymers such as pullulan.[22] Moreover, the hydrodynamic diameter of magnetic nanoparticles coated by a series of carboxymethylated polysaccharides, such as dextran, cellulose, and pullulan, were found to be 229, 719, and 330 nm, respectively.[23] The ζ potential in all of these cases had slightly negative values, which increased with increasing magnetite content (see Table I).

TGA

TGA was performed to further confirm the inclusion of the magnetite nanoparticles and to assess the content of the Fe_3O_4 incorporated into pullulan and remaining after centrifugation (see the Experimental section). Figure 9 shows the DTG curves for the native pullulan and PuF_x samples.

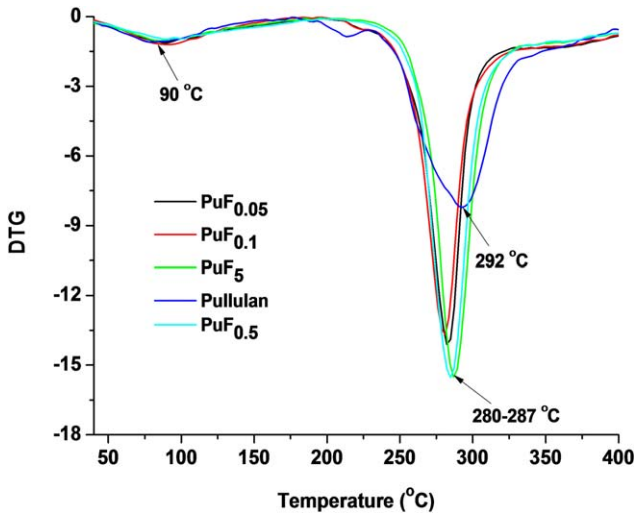

Figure 9. DTG curves of the native pullulan and PuF_x samples. [Color figure can be viewed in the online issue, which is available at wileyonlinelibrary.com.]

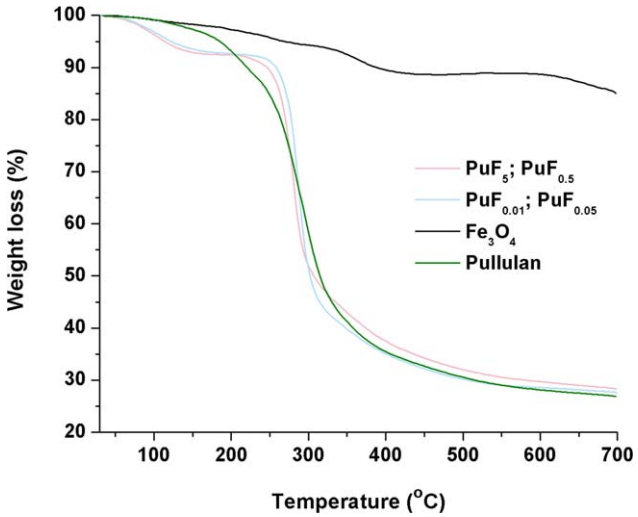

Figure 10. TGA of the naked Fe_3O_4 and PuF_x nanoparticles. [Color figure can be viewed in the online issue, which is available at wileyonlinelibrary.com.]

As the DTG curves revealed, all of the samples had maximum rates of mass loss at 280–287°C for the PuF_x samples and 292°C for the native pullulan sample. Before these temperatures, there was another small peak around 90°C, which indicated the mass loss by volatilization of the contained water in all of the samples.[24] Figure 10 shows the TGA curve of the naked Fe_3O_4 particles along with those of the pullulan and pullulan-coated magnetic nanoparticles. For the naked Fe_3O_4 particles, the initial weight loss (up to 130°C) was due to the evaporation of the adsorbed water, and the weight loss from 130 to 406°C was caused by the removal of the residual oleic acid.[25] The weight loss for the Fe_3O_4 particles in the range 25–700°C was about 15.4 wt %. In contrast, pullulan exhibited two overall weight loss steps of about 10 and 68%, respectively; these could be ascribed to the evaporation of adsorbed water (up to about 190°C) and the decomposition of the organic backbone (up to 450°C). The weight loss for pullulan was 73.45 wt %.

For the pullulan–magnetite samples, the thermogravimetric curves were very similar and made only minor differences to the weight loss. The samples PuF_5 and $PuF_{0.5}$ showed a weight loss around 72.90% because the other two samples had weight losses of 73.27%. With these data, the pullulan content in the PuF_x samples was assessed; we divided the weight loss of each sample by the weight loss of pullulan (73.45%). Therefore, the magnetite content (expressed as a percentage) was the difference between 100% and the found percentage of pullulan. The magnetite content in the PuF_x samples were in the range of 0.25% for the samples $PuF_{0.01}$ and $PuF_{0.05}$ to 0.75% for the samples $PuF_{0.1}$ and PuF_5.

The use of magnetic nanoparticles in biomedical or bioengineering applications is strongly related to their superparamagnetic character. Therefore, the magnetic properties of the as-prepared Pu-

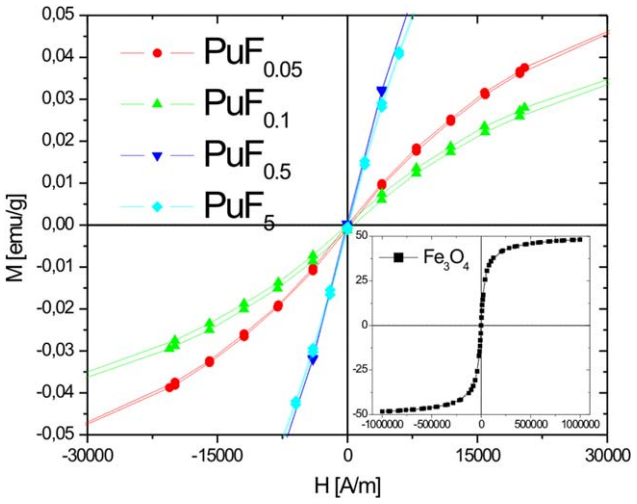

Figure 11. Magnified view (region between −300 and 300 kA/m) of the magnetization curves of the pullulan–magnetite nanoparticles. The insert shows the magnetization curve of the naked Fe_3O_4 particles. Magnetization (M), Field (F). [Color figure can be viewed in the online issue, which is available at wileyonlinelibrary.com.]

USPIO samples were investigated in a VSM system at room temperature. Figure 11 presents the magnetization curves of the Fe_3O_4 nanoparticles and Pu-USPIO samples. All of the samples showed superparamagnetism because the diameters of these samples were much lower than the critical particles size of the ferromagnetic Fe_3O_4 nanoparticles, which was 25 nm.[26] The lack of hysteresis was one of the criteria for the identification of a product with superparamagnetic properties.[12] As shown in Figure 11, the magnetization curves for all of the samples presented no hysteresis and were completely reversible at room temperature. Moreover, the superparamagnetic properties of the pullulan–magnetite samples were confirmed by the absence of coercivity and remanence.

According to the insert in Figure 11, the naked magnetite nanoparticles had a magnetization of 48 emu/g. With this value and the magnetization values of the pullulan–magnetite samples, the mass percentage of the magnetite in the pullulan-coated magnetite samples was found to be around 0.2% in samples $PuF_{0.05}$ and $PuF_{0.1}$. The magnetite percentage was three times higher for samples $PuF_{0.5}$ and PuF_5 (0.6%).

The lower values of magnetization of the PuF_x samples as compared with that of bulk magnetite were due to the high pullulan–magnetite mass ratio. However, these values were close to those reported for magnetite-decorated attapulgite (0.29 emu/g).[27]

CONCLUSIONS

Pu-USPIOs with sizes varying from 3.4 to 8.4 nm and having a core–shell structure with a magnetic core and a polymeric shell were prepared in this study. These sizes were unequivocally determined with a readily obtained pullulan–magnetite homogeneous liquid solution as a supernatant of centrifugation. When this clear, homogeneous solution was subject to solvent evaporation, transparent, light yellowish magnetic films were obtained. These films were consequently analyzed by means of AFM and SAXS when we observed that the iron nanoparticles exhibited a higher tendency to form aggregates and clusters with a mean size of 20 nm and a maximum size of 50 nm.

ACKNOWLEDGMENTS

One of the authors (V.S.) acknowledges financial support from the 2012–2015 Romanian Academy – Timisoara Branch/Centre for Fundamental and Advanced Technical Research (AR-FT/CCTFA) research program. The authors are grateful to Oana Marinica [Politehnica University of Timisoara/Research Centre of Complex Fluid Systems Engineering (RCCFSE)] for the VSM measurements.

REFERENCES

1. Singh, R. S.; Saini, K. G.; Kennedy, J. F. *Carbohydr. Polym.* **2008**, *73*, 515.
2. Coseri, S.; Spatareanu, A.; Sacarescu, L.; Rimbu, C.; Suteu, D.; Spirk, S.; Harabagiu, V. *Carbohydr. Polym.* **2014**, *116*, 9.
3. Turcheniuk, K.; Tarasevych, A. V.; Kukhar, V. P.; Boukherroub, R.; Szunerits, S. *Nanoscale* **2013**, *5*, 10729.
4. Lee, J. H.; Kim, J. W.; Cheon, J. *Mol. Cells* **2013**, *35*, 274.
5. Moghimi, S. M.; Hunter, A. C.; Murray, J. C. *Pharmacol. Rev.* **2001**, *53*, 283.
6. Stolnik, S.; Illum, L.; Davis, S. S. *Adv. Drug Delivery Rev.* **1995**, *16*, 195.
7. Raveendran, P.; Fu, J.; Wallen, S. L. *J. Am. Chem. Soc.* **2003**, *125*, 13940.
8. Yuen, S. *Process. Biochem.* **1974**, *9*, 7.
9. Kaneo, Y.; Tanaka, T.; Nakano, T.; Yamagughi, Y. *J. Controlled Release* **2001**, *70*, 365.
10. Yang, B.; Cai, H.; Qin, W.; Zhang, B.; Zhai, C.; Jiang, B.; Wu, Y. *Int. J. Nanomed.* **2013**, *8*, 3977.
11. Di Marco, M.; Sadun, C.; Port, M.; Guilbert, I.; Couvreur, P.; Dubernet, C. *Int. J. Nanomed.* **2007**, *2*, 609.
12. Zhu, A. P.; Yuan, L. H.; Liao, T. Q. *Int. J. Pharm.* **2008**, *350*, 361.
13. Li, G. Y.; Jiang, Y. R.; Huang, K. L.; Ding, P.; Chen, J. *J. Alloys Compd.* **2008**, *466*, 451.
14. Chang, P. R.; Yu, J.; Ma, X.; Anderson, D. P. *Carbohydr. Polym.* **2011**, *83*, 640.
15. Bica, D. *Rom. Rep. Phys.* **1995**, *47*, 265.
16. Vekas, L.; Bica, D.; Avdeev, M. V. *China Particuol.* **2007**, *5*, 43.
17. Avdeev, M. V.; Bica, D.; Vekas, L.; Aksenov, V. L.; Feoktystov, A. V.; Marinca, O.; Rosta, L.; Garamus, V. M.; Willumeit, R. *J. Colloid Interface Sci.* **2009**, *334*, 37.
18. Vuličević, L. J.; Ivanović, N.; Popović, N.; Novaković, M.; Popović, M.; Mitrić, M.; Andrić, V.; Babić, D. *J. Microsc.* **2008**, *232*, 629.
19. Yang, K.; Peng, H.; Wen, Y.; Li, N. *Appl. Surf. Sci.* **2010**, *256*, 3093.
20. Zhong, Z. Y.; Prozorov, T.; Felner, I.; Gedanken, A. *J. Phys. Chem. B* **1999**, *103*, 947.
21. Tombacz, E.; Bica, D.; Hajdu, A.; Illes, E.; Majzic, A.; Vekas, L. *J. Phys. Condens. Matter* **2008**, *20*, 2014103.
22. Gao, F. P.; Zhang, H. Z.; Liu, L. R.; Wang, Y. S.; Jiang, Q.; Yang, X. D.; Zhang, Q. Q. *Carbohydr. Polym.* **2008**, *71*, 606.

23. Wotschadlo, J.; Liebert, T.; Heinze, T.; Wagner, K.; Schnabelrauch, M.; Dutz, S.; Muller, R.; Steiniger, F.; Schwalbe, M.; Kroll, T. C.; Höffken, K.; Buske, N.; Clement, J. H. J. *Magn. Magn. Mater.* **2009**, *321*, 1469.

24. Gao, F.; Cai, Y.; Zhou, J.; Xie, X.; Ouyang, W.; Zhang, Y.; Wang, X.; Zhang, X.; Wang, X.; Zhao, L.; Tang, J. *Nano Res.* **2010**, *3*, 23.

25. Perez-Dieste, V.; Castellini, O. M.; Crain, J. N.; Eriksson, M. A.; Kirakosian, A.; Lin, J. L.; McChesney, J. L.; Himpsela, F. J.; Black, C. T.; Murray, C. B. *Appl. Phys. Lett.* **2003**, *83*, 5053.

26. Lee, J.; Isobe, T.; Senna, M. J. *J. Colloid Interface Sci.* **1996**, *177*, 490.

27. Liu, Y.; Liu, P.; Su, Z.; Li, F.; Wen, F. *Appl. Surf. Sci.* **2008**, *255*, 2020.